Remote Sens. **2014**, *6*, 1803-1826; doi:10.3390/rs6031803

OPEN ACCESS

remote sensing

ISSN 2072-4292

www.mdpi.com/journal/remotesensing

Article

Burned Area Detection and Burn Severity Assessment of a Heathland Fire in Belgium Using Airborne Imaging Spectroscopy (APEX)

Lennert Schepers [1,2,*], Birgen Haest [3], Sander Veraverbeke [4], Toon Spanhove [5], Jeroen Vanden Borre [5] and Rudi Goossens [2]

1 Ecosystem Management Research Group, University of Antwerp, Universiteitsplein 1, Wilrijk B-2610, Belgium

2 Department of Geography, UGent, Ghent University, Krijgslaan 281, S8, Gent B-9000, Belgium; E-Mail: Rudi.Goossens@ugent.be

3 Remote Sensing Department, Flemish Institute for Technological Research (VITO), Boeretang 200, Mol B-2400, Belgium; E-Mail: Birgen.Haest@gmail.com

4 Department of Earth System Science, UCI, University of California, Irvine, 2224 Croul Hall, Irvine 92697, CA, USA; E-Mail: sveraver@uci.edu

5 INBO, Research Institute for Nature and Forest, Kliniekstraat 25, Brussel B-1070, Belgium; E-Mails: Toon.Spanhove@inbo.be (T.S.); Jeroen.VandenBorre@inbo.be (J.V.B.)

***** Author to whom correspondence should be addressed; E-Mail: lennert.schepers@uantwerpen.be; Tel.: +32-3-265-22-52; Fax: +32-3-265-22-71.

Received: 29 December 2013; in revised form: 8 February 2014 / Accepted: 10 February 2014 / Published: 27 February 2014

Abstract: Uncontrolled, large fires are a major threat to the biodiversity of protected heath landscapes. The severity of the fire is an important factor influencing vegetation recovery. We used airborne imaging spectroscopy data from the Airborne Prism Experiment (APEX) sensor to: (1) investigate which spectral regions and spectral indices perform best in discriminating burned from unburned areas; and (2) assess the burn severity of a recent fire in the *Kalmthoutse Heide*, a heathland area in Belgium. A separability index was used to estimate the effectiveness of individual bands and spectral indices to discriminate between burned and unburned land. For the burn severity analysis, a modified version of the Geometrically structured Composite Burn Index (GeoCBI) was developed for the field data collection. The field data were collected in four different vegetation types: *Calluna vulgaris*-dominated heath (dry heath), *Erica tetralix*-dominated heath (wet heath), *Molinia caerulea* (grass-encroached heath), and coniferous woodland. Discrimination

between burned and unburned areas differed among vegetation types. For the pooled dataset, bands in the near infrared (NIR) spectral region demonstrated the highest discriminatory power, followed by short wave infrared (SWIR) bands. Visible wavelengths performed considerably poorer. The Normalized Burn Ratio (NBR) outperformed the other spectral indices and the individual spectral bands in discriminating between burned and unburned areas. For the burn severity assessment, all spectral bands and indices showed low correlations with the field data GeoCBI, when data of all pre-fire vegetation types were pooled (R^2 maximum 0.41). Analysis per vegetation type, however, revealed considerably higher correlations (R^2 up to 0.78). The Mid Infrared Burn Index (MIRBI) had the highest correlations for *Molinia* and *Erica* (R^2 = 0.78 and 0.42, respectively). In *Calluna* stands, the Char Soil Index (CSI) achieved the highest correlations, with R^2 = 0.65. In *Pinus* stands, the Normalized Difference Vegetation Index (NDVI) and the red wavelength both had correlations of R^2 = 0.64. The results of this study highlight the superior performance of the NBR to discriminate between burned and unburned areas, and the disparate performance of spectral indices to assess burn severity among vegetation types. Consequently, in heathlands, one must consider a stratification per vegetation type to produce more reliable burn severity maps.

Keywords: heathland; Composite Burn Index (CBI); GeoCBI; separability index; burn severity map; spectral indices; hyperspectral

1. Introduction

Heathlands in Europe are highly valued as habitats for biodiversity conservation, as relict landscapes of European heritage and as prime leisure areas [1–5]. Most remaining heathlands are now protected under the European Habitats Directive (92/43/EEC), the European Birds Directive (2009/147/EC), or under national legislation. Although prescribed burning is used as a management tool in many heathlands [4,6–10], uncontrolled wildfires are a major threat to heathland habitats (e.g., [1,11,12]), with potentially devastating effects. In the short-term, heath fires partially or completely remove the vegetation layer and litter [5,11], thereby destroying the typical habitats and associated fauna. In the long-term, wildfires can alter species composition and diversity [5,11,13–16]. As a result, typical heathland species, such as *Erica tetralix* and *Calluna vulgaris*, are replaced by dominant grasses, such as *Molinia caerulea* [7,12,17–19]. Important to note, these degraded heathlands become even more vulnerable to wildfires [12]: *Molinia caerulea* produces large amounts of highly flammable dead grass material, thus, risking to drag the heathland into a self-reinforcing cycle of *Molinia caerulea* establishment [11].

The severity of a fire is one of the factors controlling post-fire vegetation recovery and species composition [13,15]. In wildfire research, the terms burn severity and fire severity are often used interchangeably [20–22]. Lentile *et al.* [21], however, suggest a clear temporal distinction between both terms. Fire severity quantifies the immediate short-term fire effects on the local environment, whereas burn severity quantifies both the short and long-term impact as it includes response processes such as vegetation recovery [21,22]. In the last few decades, remote sensing techniques have emerged

in wildfire studies thanks to their: (i) synoptic overview [23–26], (ii) vast coverage [21,27–29]; and (iii) repeated temporal sampling [21,27,30]. Furthermore, (iv) remote and inaccessible parts are easily studied [21,25,31], and (v) remote sensing studies are often cheaper and faster than detailed time-consuming field campaigns [21,24,29,30]. Various methods have been developed for burn severity assessments, including spectral indices (SIs) [32], simulation techniques [28,29,33], and spectral mixture analysis [34–40]. Spectral indices are the most widely used technique, due to their conceptual simplicity and computational efficiency [41]. Many studies rely on the Normalized Difference Vegetation Index (NDVI) [42–44], which uses the absorption and reflection characteristics of plants in the R (red) and NIR (near-infrared) spectral regions respectively. Numerous modifications of the NDVI have been derived to reduce atmospheric sensitivity and background variability [41]. Other spectral indices have been developed specifically to detect post-fire effects: the Burned Area Index (BAI) [45], the Char Soil Index (CSI) [46], the Mid Infrared Burn Index (MIRBI) [47], and the Normalized Burn Ratio (NBR) [25]. Bi-temporal change detection is frequently used by differencing the post- and pre-fire index images, as this strongly reduces the spectral confusion between burned areas and spectrally similar terrain features, such as water, shadow, and dark soil [41,48]. One of these differenced SIs, the dNBR (differenced Normalized Burn Ratio), has become the standard SI approach to assess burn severity. However, bi-temporal indices do not always outperform single date indices [49,50]. In addition, the bi-temporal approach requires two images and is more constrained by, e.g., limited availability of cloud-free imagery [44,51,52], and difficulties regarding image-to-image normalization that need to be accounted for [53,54]. Therefore, Boelman *et al.* [52] and Harris *et al.* [44], among others, emphasize the utility of mono-temporal images for burn severity assessments.

Previous studies have shown that burn severity assessments in forests generally achieve better results than in low cover environments such as shrublands or grasslands [25,32,49,55,56]. Heath landscapes generally have characteristic sparse vegetation cover as well. Thus far, little is known about how conventional burn severity indices perform in these landscapes. In this study, we use airborne imaging spectroscopy data to evaluate the variety of existing indices to discriminate between burned and unburned areas and assess burn severity in the *Kalmthoutse Heide*, a protected heath landscape in Northern Belgium that was recently hit by a severe wildfire.

2. Study Area and Data

2.1. Study Area

The *Kalmthoutse Heide* is a well-documented, intensively studied, protected heath landscape in Belgium, 25 km north of Antwerp, along the border with the Netherlands (Figure 1). The 1000 ha core area consists of different heathland vegetation types [57]. Wet heath dominated by *Erica tetralix*, is endangered by encroaching grass species, most importantly *Molinia caerulea*. Dry heath, dominated by *Calluna vulgaris* vegetation, occurs on the higher zones. Sand dunes and acidic pools are scattered across the region. The inner heathland area is surrounded by coniferous woodlands (*Pinus* ssp.) and pastures. During exceptionally dry periods (often in late spring or summer) the area is prone to wildfires. In 1976 and 1996, relatively large fires destroyed parts of the nature reserve, 120 ha and 330 ha, respectively. The 2011 spring season was extremely dry and warm, causing fires in several

reserves in Belgium. On 25 and 26 May 2011, a wildfire burned 370 ha of the core heathland area of the *Kalmthoutse Heide*. This fire was the subject of our research.

Figure 1. (**a**) False color composite (RGB: LSWIR: 2332 nm; NIR: 801 nm, R: 699 nm) of the APEX image of 27 June 2011, over the *Kalmthoutse Heide*, showing the 2011 burn scar. Locations of field plots are indicated (yellow plus signs). The two north-south oriented black lines are the result of on-board calibration to measure dark current during acquisition (see Section 2.3). (**b**) pre-fire vegetation types within the burn scar (see Section 2.4).

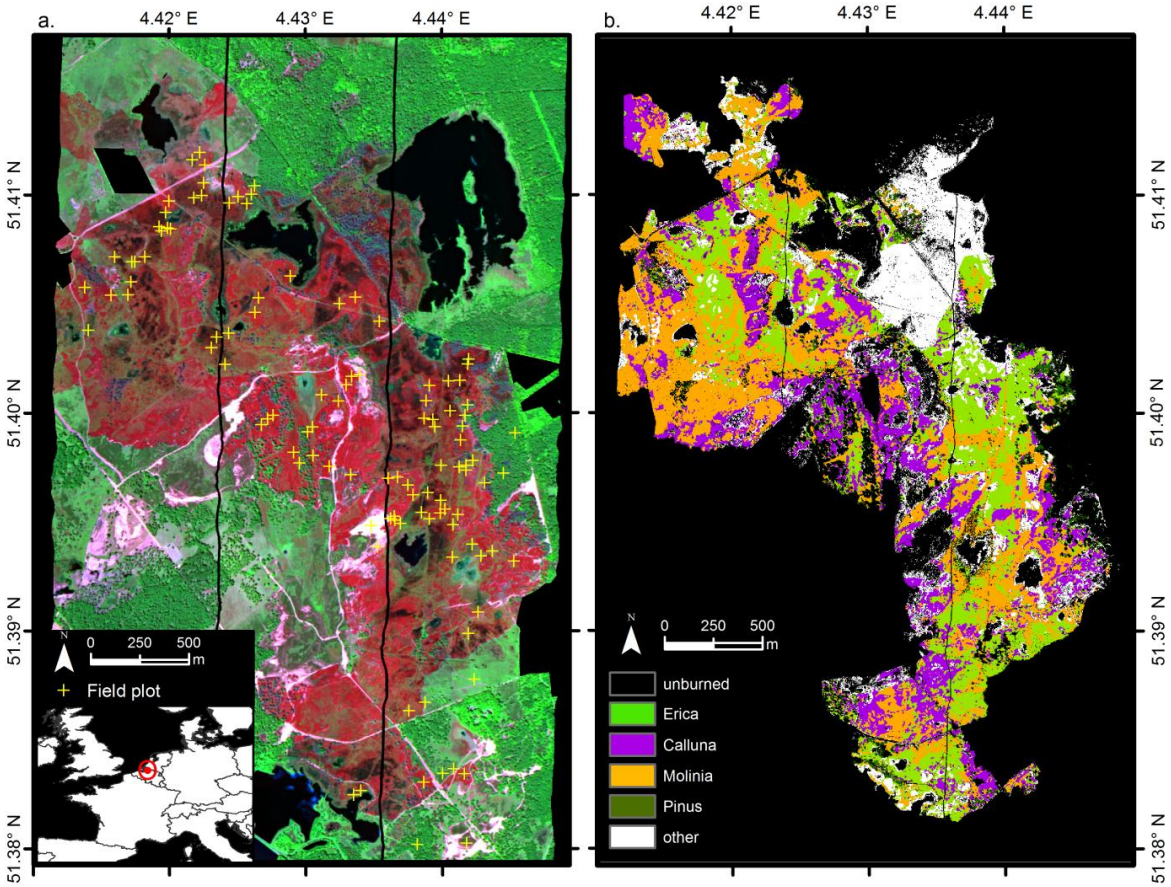

2.2. Field Data

Field measurements were collected from 10 to 12 weeks post-fire using a modified version of the Geometrically structured Composite Burn Index (GeoCBI) [56]. The GeoCBI is an adaptation of the Composite Burn Index (CBI) [25]. The GeoCBI and CBI assess several factors of burn severity in the field for five vegetation strata: (i) substrates; (ii) grasses, herbs and small shrubs below 1 m; (iii) tall shrubs and trees up to 5 m; (iv) trees from 5 to 20 m; and (v) big trees taller than 20 m. The GeoCBI differs from the CBI by including the Fraction of COVer (FCOV) of each vegetation layer and as such should better reflect the spectral mixture as perceived by remote sensing systems, resulting in higher correlations with spectral reflectance [56]. In heathland vegetation, shrubs rarely grow higher than one meter leaving only two strata to analyze. To account for the characteristics of heathland vegetation, we added and modified some factors according to field expert knowledge and literature review (Table 1). For example, we added the percentage of black char (e.g., [21,34,38,39,58]) and used the length of

burned *Calluna* branches [59] as measures of severity (Table 1). In our study area, the fifth stratum (big trees, higher than 20 m) was not present and was therefore omitted. The factor scores were rated between zero (unburned) and one (high severity) and averaged per stratum. A plot's final GeoCBI score was then calculated as the average stratum scores weighted by their FCOV:

$$\text{GeoCBI} = \frac{\sum_{m=1}^{n}(\text{CBI}_m \times \text{FCOV}_m)}{\sum_{m=1}^{n}\text{FCOV}_m} \quad (1)$$

where m refers to each vegetation stratum and n is the number of strata. CBI_m refers to the average score of stratum m.

Table 1. Modified Geometrically structured Composite Burn Index (GeoCBI) for heathlands used in this study.

Factors	Rating	Factor Score	References
A. SUBSTRATES		**Weighting Factor: 1**	
Ancillary data: Percentage dead leaves on the soil, pre-fire exposed soil			
Percentage black char	0–100%	0–1	[21,34,38,39,58]
Medium/heavy fuel charring	Light/superficial/medium/deep	0.2 / 0.4/ 0.6 / 0.8	[25]
Soil cover change	0–100%	0–1	[25]
B. MOSSES, GRASSES, HERBS, LOW SHRUBS < 1 m		**Weighting Factor: Fraction of Cover (FCOV)**	
Ancillary data: Dominant pre-fire vegetation type, dominant regrowth species, dominant sprout species			
% Foliage altered	0–100%	0–1	In contrast to [25,56], mosses and grasses are included here, since they make up a large part of the ground cover in heath landscapes (similar to [50] in tundra landscapes).
Length of burned *Calluna* branches	Average length in cm of the 3 longest burned branches in or within 1 m of the plot's border.	1–(rating/100)	Similar to shrub skeleton height [59]
Regrowth % cover	0–100%	1–(rating/% foliage altered)	This study
Sprouts	1–10	1–(rating/10)	[56]
C. TALL SHRUBS AND TREES 1–5 m (only if FCOV > 5%)		**Weighting Factor: FCOV**	
Ancillary data: Dominant vegetation type			
% Foliage altered	0–100%	0–1	[25]
Frequency % living	0–100%	1–rating	[25]
Leaf Area Index change %	0–100%	0–1	[56]
D. TREES > 5 m (only if FCOV > 5%)		**Weighting Factor: FCOV**	
Ancillary data: Dominant vegetation type			
% Green (unaltered)	0–100%	1–rating	[25]
% Black/brown	0–100%	0–1	[25]
Frequency % living	0–100%	1– rating	[25]
Leaf Area Index change %	0–100%	0–1	[25]
Char height	Average char height in meter.	rating/8 (max score 1)	[25]

In total, 109 field plots were measured (Figure 1a). In order to enable studying pre-fire vegetation type effects on the GeoCBI—SI correlations, we stratified our sample design based on four vegetation types, derived from the 2007 classification and verified with field records: *Calluna vulgaris*-dominated heath (dry heath): 34 plots, *Erica tetralix*-dominated heath (wet heath): 29 plots, *Molinia caerulea* (grass-encroached heath): 27 plots, and *Pinus* ssp. (coniferous woodland): Eight plots (Figure 2). Note that for *Erica* plots, the GeoCBI range is small, only ranging from 0.4 to 0.8 with no unburned plots. Nine plots did not belong to one of the vegetation classes.

Figure 2. Histograms of Geometrically structured Composite Burn Index (GeoCBI) scores per vegetation type with bin-width 0.2. Unburned plots have a GeoCBI score of 0, while 1 represents highest severity. The total numbers of plots (n) are given between brackets.

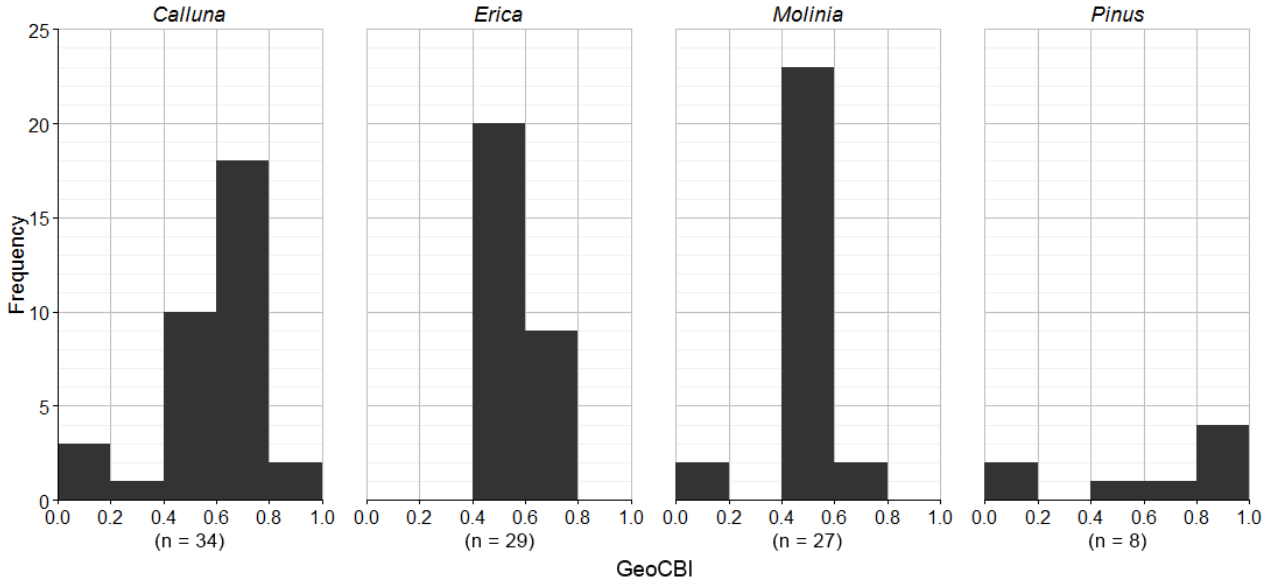

Eighty plots were sampled that were homogeneous in both pre-fire vegetation type and burn severity. In most burn severity studies, only homogeneous field plots are used [22,25,60]. As a consequence, obtained correlations are actually only truly valid for areas with relatively homogeneous burn severity, and say little about heterogeneous parts, e.g., transition areas. By including a number of plots in random locations, chances of including heterogeneous plots increase, and as such the obtained correlations should be less biased towards homogeneous areas only. For this reason, we sampled 29 additional plots, based on randomly generated coordinates. As was to be expected, these random plots were found to be more heterogeneous in terms of both burn severity and vegetation types.

Plots were located and recorded using a Real Time Kinematic Global Positioning System (RTK-GPS, Trimble GPS R6+, Trimble Navigation Limited, CA, USA) with a horizontal accuracy below 1.5 cm. Under tree canopies, where RTK-GPS signals are less strong, the accuracy remained under 0.5 m after post-processing. In each plot, the modified GeoCBI was recorded in circular plots of 4 m diameter, which is close to the 2.4 m pixel resolution of the imagery (see next paragraph). Figure 3 shows field plot examples with different burn severities in both dry heath and wet heath vegetation.

Figure 3. Example photographs and modified GeoCBI score (under each photograph) of dry (**Left**) and wet heath (**Middle**) and grass-encroached heath (**Right**) with different burn severity. (0 is unburned, while 1 represents highest severity).

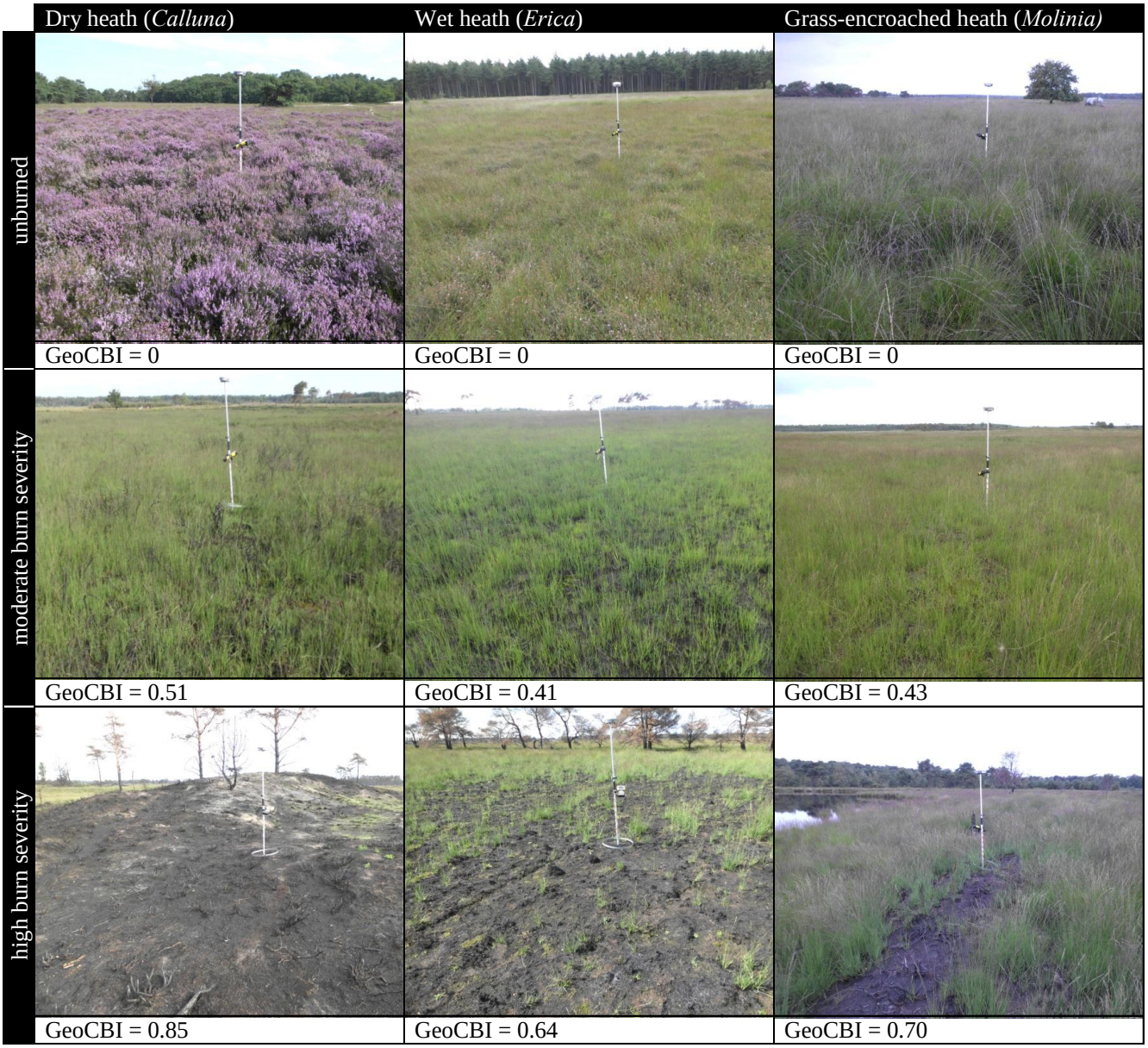

2.3. Airborne Data and Preprocessing

Airborne imaging spectroscopy data of the *Kalmthoutse Heide* were acquired on 27 June 2011, *i.e.*, approximately one month post-fire, using the Airborne Prism Experiment (APEX) sensor (Figure 1a). The sensor was operated by the Flemish Institute for Technological Research (VITO), and images were captured with a spatial resolution of 2.4 m. Spectrally, the data consisted of 288 narrow-band images, ranging from the visible to the longer shortwave infrared (LSWIR) spectral domain (410–2450 nm), with a spectral resolution between 5 nm and 10 nm [61]. Geometric, radiometric and atmospheric corrections were performed using VITO's in-house Central Data Processing Center (CDPC); as described by Biesemans *et al.* [62]. The two north-south oriented black lines visible on Figure 1a are the result of on-board calibration to measure dark current during acquisition [61]. Previous validation tests on

airborne imaging spectrometer data, acquired in similar conditions, have shown the geometric accuracy of the implemented algorithms to be at sub-pixel accuracy [62]. Atmospheric corrections are based on the radiative transfer code Modtran 4 [63]. After these corrections, the obtained data product consisted of 288 bands of reflectance images. The bands that were acquired in the atmospheric water absorption regions (881–986 nm; 1072–1176 nm; 1322–1450 nm; 1790–1969 nm) were excluded, reducing the amount of spectral bands used in the study to 223.

2.4. Ancillary Data

The *Kalmthoutse Heide* has been the subject of a five-year study (2007–2011) on mapping heathland habitat quality using airborne imaging spectroscopy. This study provided us with a thoroughly validated vegetation type classification map of June 2007, on which we based the pre-fire vegetation stratification for the field sampling (see Figure 1b). Details on the applied method and results of this vegetation type map can be found in Thoonen *et al.* [64].

Additionally, a detailed burn scar map was provided by VITO, which was produced using 0.25 cm spatial resolution, 4-band visible and near infrared (VNIR) UltraCam imagery of 2 June 2011, *i.e.*, five days after the fire event. This burn scar map was visually validated by local terrain managers. We chose to use this map to analyze performance of the spectral regions to discern between burned and unburned land because of the higher spatial detail, the closer date to the fire event, and to ensure independency of the used APEX imagery.

3. Methods

3.1. Spectral Indices

Nine widespread spectral indices for burn severity analysis were calculated in this study (Table 2), using APEX bands in five spectral regions: blue (B: 450–500 nm), red (R: 600–700 nm), near infrared (NIR: 700–1300 nm), shorter SWIR (SSWIR: 1300–1900 nm), and longer SWIR (LSWIR: 1900–2500 nm). Within each spectral region, the bands that revealed the highest discriminatory power were used to calculate the spectral indices (see Section 3.2). The NDVI is a widely used SI and is related to the amount of green vegetation making use of the relatively high reflection of vegetation in the NIR spectral region wavelengths, and absorption of radiation by chlorophyll in the red spectral region [65]. Other indices were designed to minimize the influence of disturbing signals, such as background and atmospheric effects, on the NDVI [41,66,67]. The non-linear design of the Global Environmental Monitoring Index (GEMI) strongly reduces atmospheric effects [68], which are considered very important for the remote sensing of dark surfaces such as burned areas [69]. Shorter wavelengths are more sensitive to atmospheric effects and the Enhanced Vegetation Index (EVI) uses this property by using the blue band's sensitivity to calibrate the red band [70]. Additionally, the EVI enhances the vegetation signal by decoupling the background signal from the vegetation signal with a canopy background adjustment factor that addresses non-linear, differential and red radiant transfer through a canopy [70]. The Soil Adjusted Vegetation Index (SAVI) [67] similarly adds a soil correcting factor to the formula of the NDVI to account for background effects. The calibration constant L is set to 0.5 in

this study (see Table 2) as this value is well suited for a wide range of background brightness values and vegetation densities [49,50,67].

Table 2. Spectral indices tested in this study. See text for wavelength intervals.

Spectral Index	Abbreviation	Formula	Reference
Normalized Difference Vegetation Index	NDVI	$NDVI = \frac{NIR-R}{NIR+R}$	[65]
Global Environmental Monitoring Index	GEMI	$GEMI = \gamma(1-0.25\,\gamma) - \frac{R-0.125}{1-R}$ with $\gamma = \frac{2(NIR^2-R^2)+1.5\,NIR+0.5\,R}{NIR+R+0.5}$	[68]
Enhanced Vegetation Index	EVI	$EVI = 2.5\,\frac{NIR-R}{NIR-6\,R-7.5\,B+1}$	[70]
Soil Adjusted Vegetation Index	SAVI	$SAVI = (1+L)\frac{NIR-R}{NIR+R+L}$ with $L = 0.5$	[67]
Modified Soil Adjusted Vegetation Index	MSAVI	$MSAVI = \frac{2\,NIR+1-\sqrt{(2\,NIR+1)^2-8\,(NIR-R)}}{2}$	[66]
Burned Area Index	BAI	$BAI = \frac{1}{(0.1+R)^2+(0.06+NIR)}$	[45]
Normalized Burn Ratio	NBR	$NBR = \frac{NIR-LSWIR}{NIR+LSWIR}$	[25]
Char Soil Index	CSI	$CSI = \frac{NIR}{LSWIR}$	[46]
Mid-Infrared Burn Index	MIRBI	$MIRBI = 10\,LSWIR - 9.8\,SSWIR + 2$	[47]

Notes: B: Blue, R: Red, NIR: Near Infrared, SSWIR: Shorter Short Wave Infrared, LSWIR: Longer Short Wave Infrared.

Qi *et al.* [66] elaborated on the SAVI and designed the Modified Soil Adjusted Vegetation Index (MSAVI), which automatically sets the calibration constant based on vegetation density to further reduce the background noise. The Burned Area Index (BAI) was specifically designed to detect and enhance the char signal [45]. The BAI uses red and NIR reflectance values to calculate the spectral distance from each pixel to a reference spectral point to which burned pixels converge. The spectral values of this reference point (NIR reflectance 0.06 and R reflectance 0.1) were based on literature and analysis of several sets of satellite sensor images [45]. The Normalized Burn Ratio (NBR) [25] uses the Near Infrared (NIR) and Longer Short Wave Infrared (LSWIR) spectral region instead of the R region as used by the NDVI. In the LSWIR region radiation is strongly absorbed by the water content in vegetation or soils [25]. Scorching, drying, or dry soil exposure after fire will increase the LSWIR reflection and thereby decrease the NBR value [25,71]. The CSI similarly makes use of this feature by rationing the NIR and the LSWIR reflectance values [46]. The MIRBI [47] was designed for a shrub-savannah vegetation type, where NIR wavelengths are less useful due to the senescent state of the vegetation in the fire season. The index was developed in a Shorter Short Wave Infrared (SSWIR)/LSWIR spectral space and its performance was proven to be relatively stable over time in savannah ecosystems [47].

3.2. Spectral Sensitivity for Burned Area Discrimination

A separability index (Equation (2)) was used to estimate the effectiveness of (i) individual bands and (ii) spectral indices to discriminate between burned and unburned land. The separability index

(also called normalized distance) has been used before to assess the power of mostly broadband sensors to discriminate burned areas [41,46,69,71–73], and was chosen for its widespread use in fire studies. The separability index is computed as follows:

$$M = \frac{|\mu_b - \mu_u|}{\sigma_b + \sigma_u} \quad (2)$$

where μ_b and μ_u are the mean values of the considered spectral band of the burned and unburned areas respectively, and σ_b and σ_u the corresponding standard deviations. The higher the separability index M, the better the discrimination. Values of M higher than one indicate good separability, while values lower than one represent a large degree of histogram overlap between the burned and unburned classes [41,69]. The heathland in this study is a mixture of different vegetation types (see Section 2.1 for a description). Therefore, the sensitivity analysis was performed on four vegetation types separately, based on the classification of Thoonen *et al.* [64] (Figure 1b). The bands that revealed the highest discriminatory power on the pooled dataset within each spectral region (see Section 3.1 for wavelength intervals) were used to calculate the spectral indices (Table 2).

3.3. Relationship between Spectral Bands and Indices versus Burn Severity

A linear regression analysis was applied on the GeoCBI scores of the field plots to evaluate the performance of the individual spectral bands and the SIs to assess burn severity. The correlation is defined by the coefficient of determination (R^2), *i.e.*, the proportion of total variance in the GeoCBI scores that is explained by the spectral band or SI, and statistical significance was quantified by the p-value using the F-statistic.

Previous research demonstrated that the performance of spectral indices depends on the vegetation type [32,43,49,55,74,75]. Therefore, we performed our analysis per vegetation type, as well as for all the data pooled together over the vegetation types.

Finally, a spatial distribution of the burn severity at the *Kalmthoutse Heide* was produced by using the optimal regression parameters of the four vegetation types considered in our study. For areas with other vegetation types (Figure 1b), the best performing SI for the pooled dataset was used. The area and percentage of each vegetation type within the burn scar are listed in Table 3.

Table 3. Area and percentage of each vegetation type within the burn scar. Areas not belonging to one of the four vegetation types are grouped in "other".

Vegetation Type	Area (ha)	Percentage
Erica	88.9	25.2
Calluna	72.4	20.6
Molinia	105.5	30.0
Pinus	9.0	2.6
other	76.3	21.7

4. Results

4.1. Spectral Sensitivity for Burned Area Discrimination

The bands with the highest separability index M for each spectral region are listed in Table 4. For the pooled dataset, the NIR spectral region had the highest overall M-score (M = 0.73). The LSWIR (M = 0.50) and SSWIR (M = 0.43) regions demonstrated moderate discriminatory power. The G (M = 0.22), R (M = 0.18) and, especially, the B (M = 0.05) wavelengths had very low M-values. The visible regions thus have very poor and the SWIR spectral regions moderate discriminatory power, but the best distinction is made by the NIR spectral region.

Table 4. Maximum separability index values to discern burned and unburned areas for each spectral region, both for pooled data and for each vegetation type separately. The corresponding Airborne Prism Experiment (APEX) bands (central wavelength in nm) are given between brackets. Values higher than one are given in bold.

Spectral Region	Pooled Dataset	*Calluna*	*Erica*	*Molinia*	*Pinus*
B	0.05 (499)	0.17 (450)	0.32 (499)	0.20 (499)	0.06 (450)
G	0.22 (552)	0.25 (552)	0.65 (552)	0.51 (552)	0.21 (546)
R	0.18 (699)	0.39 (699)	0.64 (699)	0.46 (699)	0.19 (675)
NIR	0.73 (801)	**1.14 (1063)**	**1.18 (828)**	**1.13 (1063)**	0.84 (767)
SSWIR	0.43 (1302)	0.98 (1302)	0.98 (1302)	**1.03 (1302)**	0.48 (1302)
LSWIR	0.50 (2232)	0.85 (2352)	0.37 (2332)	0.50 (2339)	0.43 (1977)

Note: B: Blue, G: Green, R: Red, NIR: Near Infrared, SSWIR: Shorter Short Wave Infrared, LSWIR: Longer Short Wave Infrared, see Section 3.1 for wavelength intervals.

This conclusion holds when stratifying the data, although considerable differences are present between vegetation types. The heather vegetation types (*Calluna*, *Erica*, and *Molinia*) had higher separability indices (up to M = 1.18 for the NIR band in *Erica* vegetation) than the *Pinus* vegetation, which had similar results to the pooled dataset (Table 4). The SSWIR spectral region had high M-values for the heather types (M = 0.98 and 1.03). The LSWIR region performed well (M = 0.85) in dry heath (*Calluna*), whereas this spectral region performed only moderate in *Erica* and *Molinia* vegetation types (M = 0.37 and 0.50 respectively). The optimal spectral bands of the heather species were located close to the bands of the pooled dataset, except for the NIR, the region with the highest separability index. *Pinus* vegetation had different optimal bands for most spectral regions.

The SIs were calculated with the bands of the pooled dataset (Table 2), and are listed in Table 5. Among the SIs analyzed, The NBR provided the highest discriminating ability and is the only SI with a separability index higher than one (M = 1.15). The NDVI, GEMI, SAVI, MSAVI, and MIRBI had M-values between 0.5 and 1. The BAI revealed a poorer performance (M = 0.34), and the CSI (M = 0.04) and EVI (M = 0.01) revealed very little discriminatory power.

Table 5. Separability index values to discern burned and unburned areas for the spectral indices by using the best performing bands on the pooled dataset (Table 4). Full names are listed in Table 2. Values higher than one are given in bold.

Spectral Index	Separability Index M
NDVI	0.59
GEMI	0.67
EVI	0.01
SAVI	0.74
MSAVI	0.73
BAI	0.34
NBR	**1.15**
CSI	0.04
MIRBI	0.86

4.2. Relationship between Spectral Indices and Field Assessments of Burn Severity

In general, the individual spectral bands had low correlations with the GeoCBI field data (Table 6). The SSWIR spectral band obtained the highest correlation (R^2 = 0.41) for the pooled data, the NIR band showed a slightly lower correlation (R^2 = 0.40). The other bands demonstrated R^2 values smaller than 0.2. There is a remarkable large discrepancy between the correlations of the different vegetation types. Burn severity in *Calluna* vegetation had a strong correlation with the LSWIR region (R^2 = 0.51). *Erica* vegetation in contrast did not demonstrate significant relationships in any spectral region. A strong and significant relationship was measured between the GeoCBI scores and the SSWIR band for *Molinia* vegetation (R^2 = 0.75). The *Pinus* stands revealed the highest correlation with the red spectral band (R^2 = 0.64).

The results of the correlation analysis with the SIs were comparable to the correlation analysis with the spectral bands in the sense that poor correlations were observed with pooled data, while clearly stronger relationships existed per vegetation type (Table 6). The MSAVI and MIRBI explained most of the variance for the pooled data, with an R^2 of 0.40 for both indices. Note, that for pooled data, the SSWIR spectral band (R^2 = 0.41; Table 6) gave a higher correlation than any SI. By stratifying the data per vegetation type, the correlations clearly increased. *Calluna* had the highest correlation with the CSI (R^2 = 0.65). The MIRBI, NBR, and SAVI were also suitable in *Calluna* stands. In *Erica* stands, the correlations remained relatively low, however, MIRBI showed the highest correlation coefficient (R^2 = 0.42), followed by the NDVI (R^2 = 0.38). Relatively high correlations were obtained for *Molinia* vegetation with MIRBI having the highest R^2 value (0.78). The GeoCBI of *Pinus* stands revealed strong relationships with indices that generally performed poorer in other vegetation types: the NDVI, SAVI and GEMI had the strongest correlations of 0.64, 0.63 and 0.59 respectively.

Figure 4 demonstrates how the slope of the MIRBI regression lines clearly varies per vegetation type. Consequently, using the regression line obtained for the pooled data would imply a strong generalization and loss of information.

Table 6. Relationship (expressed as R^2) between the GeoCBI field data and spectral bands and spectral indices (Table 2) with pooled data and data per vegetation type.

R^2	Pooled Data (n = 109)	Per Vegetation Type			
		Calluna (n = 34)	*Erica* (n = 29)	*Molinia* (n = 27)	*Pinus* (n = 8)
B	0.12 ***	0.21 **	0.03	0.08	**0.45**
G	0.20 ***	0.00	0.00	0.31 **	0.02
R	0.20 ***	0.05	0.03	0.33 **	**0.64 ***
NIR	**0.40 *** **	**0.41 *** **	0.13	**0.55 *** **	**0.54 ***
SSWIR	**0.41 *** **	**0.41 *** **	0.08	**0.75 *** **	0.13
LSWIR	0.00	**0.51 *** **	0.06	0.17 *	0.19
NDVI	0.14 ***	**0.49 *** **	**0.38 *** **	0.15 *	**0.64 ***
GEMI	0.21 ***	**0.45 *** **	0.15 *	**0.45 *** **	**0.59 ***
EVI	0.07 **	0.33 ***	0.14 *	**0.60 *** **	**0.44**
SAVI	0.24 ***	**0.50 *** **	0.22 **	**0.40 *** **	**0.63 ***
MSAVI	**0.40 *** **	**0.41 *** **	0.13	**0.55 *** **	**0.54 ***
BAI	0.26 ***	0.32 ***	0.10	0.31 **	**0.39**
NBR	0.22 ***	**0.55 *** **	0.25 **	**0.38 *** **	0.33
CSI	0.18 ***	**0.65 *** **	0.26 **	**0.57 *** **	**0.50**
MIRBI	**0.40 *** **	**0.58 *** **	**0.42 *** **	**0.78 *** **	0.19

Notes: n: number of field plots; *** $p < 0.001$; ** $p < 0.01$; * $p < 0.05$; no asterisk: $p > 0.05$; values higher than 0.35 are given in bold.

Figure 4. Scatter plots and linear regression lines between the Mid-Infrared Burn Index (MIRBI) and the Geometrically structured Composite Burn Index (GeoCBI) field data, for pooled data and for separate data per vegetation type.

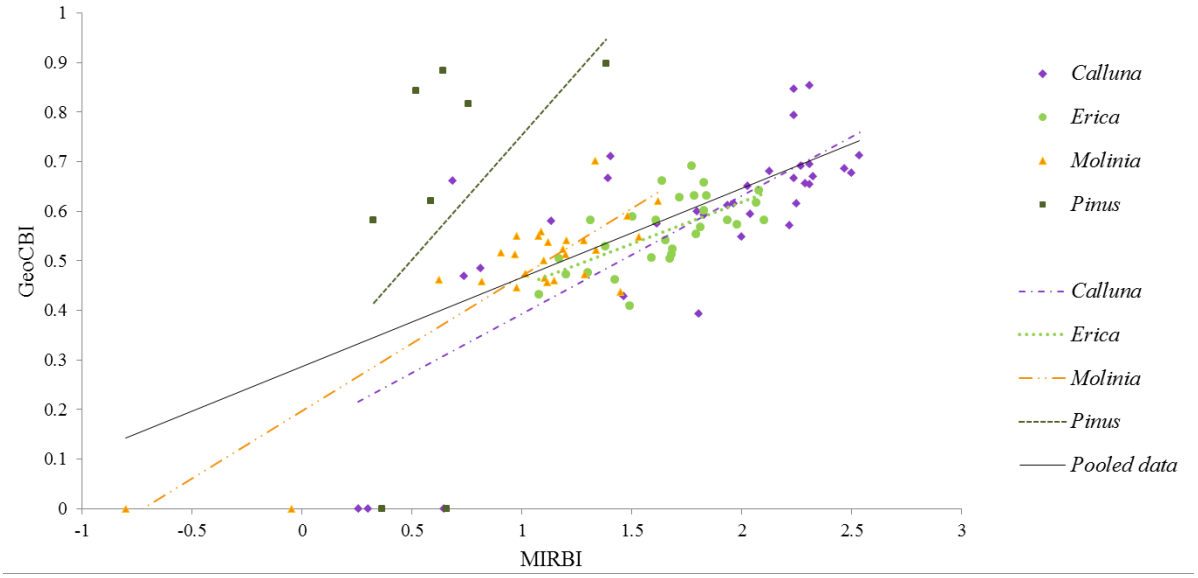

To benefit from the relatively strong correlations that were observed among the vegetation types with different SIs, the final burn severity distribution (Figure 5) combines the GeoCBI values derived

from separate regression models for each vegetation type, based on the regression parameters of the best-performing SI (Table 7). For areas not belonging to one of the four vegetation types, the regression parameters of the best performing SI on the pooled dataset were used (*i.e.*, MSAVI). This spatial distribution is expressed in GeoCBI values (Figure 5).

Table 7. Best performing spectral index and corresponding regression parameters, as used in the burn severity spatial distribution (Figure 5).

Regression Parameters		**GeoCBI = a SI + b**	
Vegetation Type	**Best Performing SI**	**Slope**	**Intercept**
Calluna	CSI	−0.2168	0.7640
Erica	MIRBI	0.1686	0.2815
Molinia	MIRBI	0.2716	0.1977
Pinus	NDVI	−1.7498	1.3697
Other classes	MSAVI	−1.9697	0.7492

Figure 5. Burn severity spatial distribution of the 2011 fire at the *Kalmthoutse Heide*, produced by using the optimal regression parameters per vegetation type (see Table 7). The burn severity is expressed in GeoCBI.

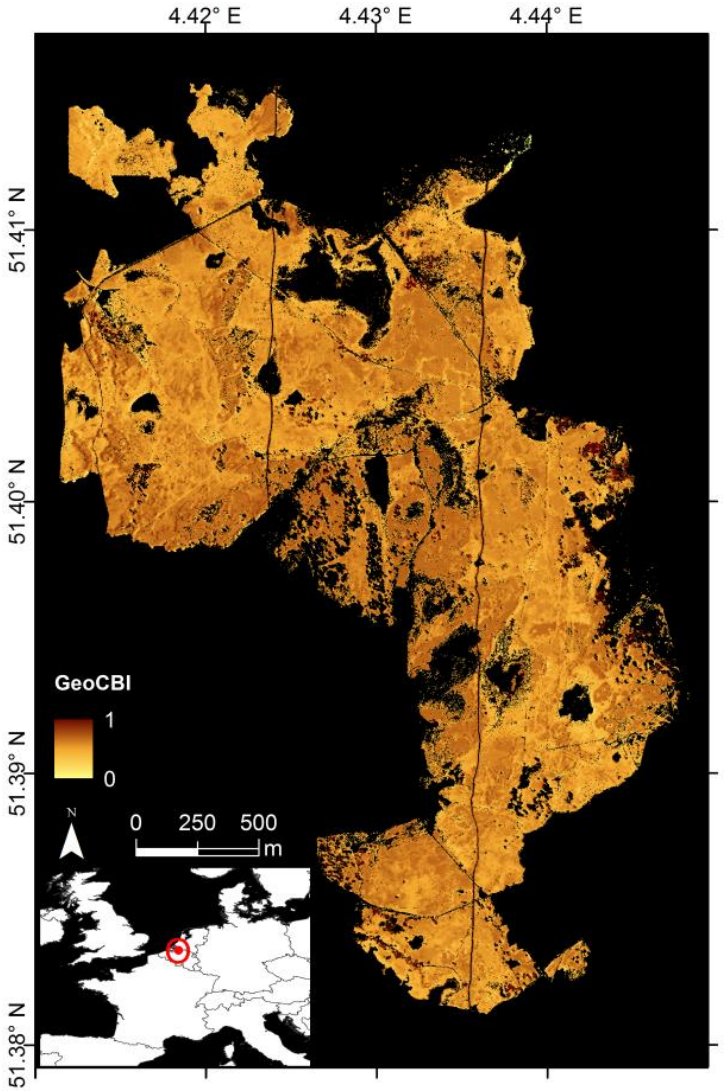

5. Discussion

5.1. Burned Area Discrimination

The high discriminatory power of the NIR spectral band is consistent with findings of Veraverbeke *et al.* [41], Smith *et al.* [46], Pereira [69], Lasaponara [73], and López-García and Caselles [76]. This spectral region has been widely considered as the best spectral region to detect and map burned areas [41,69,76,77]. The NIR region is strongly reflected by vegetation. As a result, vegetation removal or scorching implicates a post-fire drop of NIR reflectance. The SWIR reflectance increases after burning, due to the fire's removal of water-retaining vegetation [25,41]. This reflectance increase is higher than in the visible wavelengths (VIS) and, hence, the SWIR region outperforms the VIS regions. As stated in literature (e.g., [41,69,76,77]), the VIS wavelengths have a very low performance in discriminating between burned and unburned areas. A likely explanation is that water, water-rich swamps, dense conifer forests and peat soil types all are relatively dark which causes spectral confusion with burned areas in these wavelengths [69]. Differences in separability performance among wildfires have been observed by Lasaponara [73]. Lasaponara [73] suggests that these observations might be due to the different land cover types affected by the fire. Our results support the hypothesis that differences in separability performance are caused by different vegetation types within the burn scar.

The best performing LSWIR band (central wavelengths 2332, 2339, and 2352 nm, except for *Pinus*) corresponds with the findings of van Wagtendonk *et al.* [26], Veraverbeke *et al.* [41], and Pleniou and Koutsias [71], who found the most discriminating wavelengths at 2370 nm, 2310–2360 nm and 2300–2370 nm, respectively. In the study by van Wagtendonk *et al.* [26], the 788 nm NIR band demonstrated the strongest reflectance decrease, close to the optimal NIR band for *Pinus* vegetation (767 nm) and for the pooled dataset (801 nm) found in our study. The optimal SSWIR band in this study (1302 nm), however, differs with Veraverbeke *et al.* [41] (1600 nm) and van Wagtendonk *et al.* [26] (1762 nm).

The NBR had the highest discriminating power in our study, due to its combining of the spectral regions with strongest decrease and increase, the NIR and LSWIR region, respectively [26]. This index provided also good discriminatory power in South African savannahs [46]. The CSI, though using the same bands, performs poorly in this study, just as in Veraverbeke *et al.* [41]. In savannahs, however, the CSI attained a high degree of spectral separability [46]. The higher discriminative power that we found of the NIR spectral band compared to the NDVI is caused by the very low performance of the red (and visible) wavelengths. This is also confirmed by other studies, where the NIR channel alone achieved better separability results than indices based on a combination of NIR and VIS spectral bands [46,69].

5.2. Burn Severity Assessment

Very few studies analyze the correlation between separate spectral bands and field data. Epting *et al.* [49] and Hoy *et al.* [50] only report the NIR and LSWIR spectral region in their analysis. Epting *et al.* [49] analyzed correlations between the NIR-band and the GeoCBI for four forest fires, resulting in correlations (R^2) between 0.06 and 0.62. This is consistent with Hoy *et al.* [50] (R^2 = 0.39 and 0.27) and our study (R^2 = 0.40). Hoy *et al.* [50] did analyze the SSWIR band, but did not report numbers due to insignificance of the results. In our study, however, this band demonstrated the highest

correlation with the GeoCBI. For the LSWIR spectral region, we found similar results as Hoy *et al.* [50]: in both studies the LSWIR performance is very low. Epting *et al.* [49], however, revealed a R^2 between 0.19 and 0.55 for the LSWIR region. The difference in performance between the SSWIR and LSWIR spectral band might be explained by differences in liquid water absorption: water absorption in the LSWIR band is significantly stronger than in the SSWIR band [78,79]. The 1302 nm SSWIR band used in this study is situated close to the NIR spectral region. Therefore this SSWIR band is expected to be less sensitive to moisture content than to vegetation structure, which is the most important variable influencing the NIR spectral region [80,81]. The inconsistencies between the study of Hoy *et al.* [50], and Epting *et al.* [49], and this study may be due to the different ecosystems and vegetation types observed, *i.e.*, Alaskan black spruce forests, interior Alaskan vegetation types (forests, as well as low cover sites) and Atlantic European heathlands respectively.

Indeed, previous research demonstrated that the correlation performance of the GeoCBI depends on the vegetation type [32,43,49,55,74,75]. Stratifying our data per vegetation type also improved the correlation results considerably. Most studies show stronger correlations in forested areas than in sparser vegetation types like shrubs and herbs: Epting *et al.* [49] found strong relations in mixed forests ($R^2 = 0.83$). Herbs and shrubs on the other hand, showed a Pearson correlation coefficient of 0.33 and 0.25 respectively ($R^2 = 0.11$ and 0.06). The authors conclude that the CBI may not be appropriate to assess burn severity in non-forested areas. In addition, Key and Benson [25], Veraverbeke *et al.* [55], De Santis and Chuvieco [56], and the review by French *et al.* [32], show stronger correlations in forested areas than in shrub and herb vegetation. In our heathland fire study, the NBR performed rather poorly, while in other studies this index generally acquires the best results when compared to other indices [44,49,50]. This also indicates that the performance of burn severity assessment varies among vegetation types.

The CSI was the best index in dry heath (*Calluna*) vegetation. The CSI is the ratio of the NIR and LSWIR spectral band (Table 2), a low CSI value means a high burn severity. Bare soil that was exposed post-fire also results in low CSI values, due to similar reflectance values in the NIR and LSWIR region. The CSI is designed to detect the char signal [46], but it also amplifies the soil cover change signal. This results in good performances in our dry heath vegetation, as well as in the chaparral ecosystems of California [44]. Wet heath vegetation shows a very poor correlation, considerably lower than the other vegetation types. This might be partly explained by the fact that this is the only vegetation for which we did not sample unburned field plots (Figure 2), which considerably lowers the range of variability in both the SIs and GeoCBI scores, affecting the strength of the regressions. In wet heath vegetation (mainly *Erica*) and grass-encroached heath (*Molinia* stands), the MIRBI showed the best correlation with the field data. Our finding that the MIRBI had the highest correlation within the wet heath and grass vegetation types is consistent with Trigg and Flasse [47]. In fact, this SI was designed for shrub-savannah ecosystems which has similarities with heath ecosystems. For example, grasses are widely present in both ecosystems and they are both characterized by quick post-fire recovery. The relatively high correlations with the SSWIR and especially the LSWIR spectral regions indicate that the post-fire decrease in moisture content varies among and is related to different severity levels. The coniferous vegetation has the highest correlation with the red spectral band and the NDVI. Differences in severity between the coniferous woodland plots were expressed as the amount of scorching of the needles in the crown. In none of the plots the pine needles were completely burned, but the amount of scorching of the crown significantly differed

among the coniferous woodland plots. This scorching influenced the photosynthetic activity and the amount of healthy vegetation of the trees, which is measured in the red and NIR region, respectively. This might explain the superior performance of the red region and NDVI for the coniferous woodland plots. The LSWIR region in post-fire environments is especially sensitive to increased reflectance due to the charcoal signal. However, in the coniferous woodland plots, charcoal exposure remained relatively limited, which might explain the lower performance of this region. Consequently, the most important factor in this vegetation type is not the change in water content, such as in *Molinia* and *Erica* vegetation types, but the change in photosynthetically active vegetation density.

We observed a discrepancy between the results of the spectral sensitivity analysis for burned area discrimination and the burn severity regression analysis. In the burn severity analysis, the SSWIR band showed the best performance and the LSWIR band the lowest. However, the SSWIR-band resulted in low discriminatory power for burned area discrimination, while the LSWIR was the second best burned area discriminator (compare Table 6 with Table 4). The results of the spectral indices further confirm this discrepancy: the NBR outperformed the other indices in discriminating between burned and unburned areas, but was for no vegetation type the best predictor of burn severity. The opposite was also true: the CSI revealed very low discriminatory power for burned area mapping, whereas this index performed best to estimate burn severity in dry heath vegetation. Certain individual bands and indices, thus, performed differently for mapping burned area, compared to burn severity. Therefore, it is recommended to optimize the SI selection for each application separately.

We used the optimal regression parameters of the best-performing SI for each vegetation types to predict a spatial burn severity distribution for the entire burned area. An alternative approach could have been to validate the optimal regression parameters with independent field data. Due to the low number of field plots after stratification per vegetation type (e.g., eight *Pinus* plots), this was not feasible in our research.

In this study, we used spectral indices for their conceptual simplicity and computational efficiency. These spectral indices are widely used, and therefore direct comparison with previous research and other study areas is straightforward. Hence, spectral indices have clear advantages over other burn severity assessment methodologies. However, spectral indices use only a small fraction of the information contained in the spectroscopy images. For example, the spectral indices in this study used two or three spectral bands (see Table 2), whereas the APEX image acquired data in 233 bands suitable for analysis. Therefore, future research can focus on upcoming but more advanced methodologies that combine all information available from the spectroscopy data cube. Testing multiple band combinations with feature selection methods is one of the methods that may reveal more insights in the relation between severity and spectral response. Another technique that is often applied on imaging spectroscopy datasets is Spectral Mixture Analysis (SMA). SMA may reveal the proportion and physical presence of char within a pixel, which has been proposed as an indicator for severity assessments by several authors [21,34,39,58,82]. However, also these techniques have their limitations, e.g., the definition of the endmembers [83].

This article is a contribution to spectral imaging spectroscopy research of wildfires. More available spectral libraries (e.g., the ASTER spectral library [84]), new emerging SMA techniques [83] and spaceborne imaging spectroscopy missions planned in the near-future (Hyperspectral Infrared Imager, hyspiri.jpl.nasa.gov; Precursore Iperspettrale (Hyperspectral Precursor), www.isa.it; Environmental

Mapping and Analysis Program, www.enmap.org), might make spectroscopy data more widely available. This will foster more research on the spectral properties of post-fire landscapes and vegetation recovery in various vegetation types such as the heathlands in this study.

6. Conclusion

This study analyzed (i) the performance of single spectroscopy bands and spectral indices to discriminate between burned and unburned areas, and (ii) the potential of using spectroscopy bands and spectral indices and a modified version of the GeoCBI for the assessment of burn severity in a mixed heath landscape, similar to burn severity analysis in forest areas. Discrimination between burned and unburned areas differed among vegetation types. The NBR, widely applied for burn severity assessments, was the best discriminator between burned and unburned areas, and could, thus, be used in our heathland area to delineate the burn scar. For burn severity assessments, a few modifications of the GeoCBI suffice to collect severity data in the field. Using a single SI for all vegetation types within a heathland however seems undesirable, as much higher correlations with field reference data are obtained when separate spectral indices are used per pre-fire vegetation type. As a consequence, burn severity maps should ideally discriminate between vegetation types. This study is one of the first post-fire remote sensing studies performed in heathland habitats, and its repeatability and the performance of specific SIs need to be confirmed in future studies.

Acknowledgments

We thankfully acknowledge the funding for this research received from the Belgian Science Policy Office in the frame of the Stereo II program (HeathReCover project—Contract SR/67/148). We also thank the site's management bodies (Agency for Nature and Forest, and Cross-Border Park De Zoom-Kalmthoutse Heide) for granting access and for sharing their data and knowledge on the site. We would like to thank the anonymous reviewers for their helpful comments and suggestions, which have improved the quality of the manuscript.

Author Contributions

All authors contributed to the study design. Lennert Schepers, Birgen Haest and Toon Spanhove were involved in data collection. Lennert Schepers, Birgen Haest and Sander Veraverbeke conducted the data analysis. All authors contributed to manuscript writing.

Conflicts of Interest

The authors declare no conflict of interest.

References

1. De Blust, G. Heathland, an Ever Changing Landscape. In *Europe's Living Landscape. Essays Exploring Our Identity in the Countryside*; Pedroli, B., Van Doorn, A., De Blust, G., Paracchini, M.L., Wascher, D., Bunce, F., Eds.; KNNV & Landscape Europe: Zeist, The Netherlands, 2007; pp. 179–192.

2. De Blust, G.; Slootmaekers, M. *De Kalmthoutse Heide*; Davidsfonds: Leuven, Belgium, 1997.
3. Webb, N.R. The traditional management of European Heathlands. *J. Appl. Ecol.* **1998**, *35*, 987–990.
4. Davies, G.M.; Smith, A.A.; MacDonald, A.J.; Bakker, J.D.; Legg, C.J. Fire intensity, fire severity and ecosystem response in heathlands: Factors affecting the regeneration of Calluna vulgaris. *J. Appl. Ecol.* **2010**, *47*, 356–365.
5. Harris, M.P.K.; Allen, K.A.; McAllister, H.A.; Eyre, G.; Le Duc, M.G.; Marrs, R.H. Factors affecting moorland plant communities and component species in relation to prescribed burning. *J. Appl. Ecol.* **2011**, *48*, 1411–1421.
6. Ross, S.; Adamson, H.; Moon, A. Evaluating management techniques for controlling Molinia caerulea and enhancing Calluna vulgaris on upland wet heathland in Northern England, UK. *Agric. Ecosyst. Environ.* **2003**, *97*, 39–49.
7. Marrs, R.H.; Phillips, J.D.P.; Todd, P.A.; Ghorbani, J.; Le Duc, M.G. Control of Molinia caerulea on upland moors. *J. Appl. Ecol.* **2004**, *41*, 398–411.
8. Ascoli, D.; Beghin, R.; Ceccato, R.; Gorlier, A.; Lombardi, G.; Lonati, M.; Marzano, R.; Bovio, G.; Cavallero, A. Developing an adaptive management approach to prescribed burning: A long-term heathland conservation experiment in north-west Italy. *Int. J. Wildland Fire* **2009**, *18*, 727–735.
9. Velle, L.G.; Nilsen, L.S.; Vandvik, V. The age of Calluna stands moderates post-fire regeneration rate and trends in northern Calluna heathlands. *Appl. Veg. Sci.* **2012**, *15*, 119–128.
10. Goldammer, J.G.; Hoffmann, G.; Bruce, M.; Kondrashov, L.; Verkhovets, S.; Kisilyakhov, Y.K.; Rydkvist, T.; Page, H.; Brunn, E.; Lovén, L.; *et al.* The Eurasian Fire in Nature Conservation Network (EFNCN): Advances in the Use of Prescribed Fire in Nature Conservation, Landscape Management, Forestry and Carbon Management in Temperate-Boreal Europe and Adjoining Countries in Southeast Europe, Caucasus. In Proceeding of 4th International Wildland Fire Conference, Sevilla, Spain, 13–17 May 2007.
11. Brys, R.; Jacquemyn, H.; de Blust, G. Fire increases aboveground biomass, seed production and recruitment success of Molinia caerulea in dry heathland. *Acta Oecol.* **2005**, *28*, 299–305.
12. Jacquemyn, H.; Brys, R.; Neubert, M.G. Fire increases invasive spread of Molinia caerulea mainly through changes in demographic parameters. *Ecol. Appl.* **2005**, *15*, 2097–2108.
13. Díaz-Delgado, R.; Lloret, F.; Pons, X. Influence of fire severity on plant regeneration by means of remote sensing imagery. *Int. J. Remote Sens.* **2003**, *24*, 1751–1763.
14. Turner, M.G.; Romme, W.H.; Gardner, R.H. Prefire heterogeneity, fire severity, and early postfire plant reestablishment in subalpine forests of Yellowstone National Park, Wyoming. *Int. J. Wildland Fire* **1999**, *9*, 21–36.
15. Epting, J.; Verbyla, D. Landscape-level interactions of prefire vegetation, burn severity, and postfire vegetation over a 16-year period in interior Alaska. *Can. J. For. Res.* **2005**, *35*, 1367–1377.
16. Lentile, L.B.; Smith, F.W.; Shepperd, W.D. Patch structure, fire-scar formation, and tree regeneration in a large mixed-severity fire in the South Dakota Black Hills, USA. *Can. J. For. Res.* **2005**, *35*, 2875–2885.
17. El-Kahloun, M.; Boeye, D.; Verhagen, B.; van Haesebroeck, V. A comparison of the nutrient status of Molinia caerulea and neighbouring vegetation in a rich fen. *Belg. J. Bot.* **2000**, *133*, 91–102.

18. Milligan, A.L.; Putwain, P.D.; Cox, E.S.; Ghorbani, J.; Le Duc, M.G.; Marrs, R.H. Developing an integrated land management strategy for the restoration of moorland vegetation on Molinia caerulea-dominated vegetation for conservation purposes in upland Britain. *Biol. Conserv.* **2004**, *119*, 371–385.
19. Milligan, A.L.; Putwain, P.D.; Marrs, R.H. A field assessment of the role of selective herbicides in the restoration of British moorland dominated by Molinia. *Biol. Conserv.* **2003**, *109*, 369–379.
20. Keeley, J.E. Fire intensity, fire severity and burn severity: A brief review and suggested usage. *Int. J. Wildland Fire* **2009**, *18*, 116–126.
21. Lentile, L.B.; Holden, Z.; Smith, A.M.S.; Falkowski, M.; Hudak, A.; Morgan, P.; Lewis, S.; Gessler, P.; Benson, N. Remote sensing techniques to assess active fire characteristics and post-fire effects. *Int. J. Wildland Fire* **2006**, *15*, 319–345.
22. Veraverbeke, S.; Lhermitte, S.; Verstraeten, W.W.; Goossens, R. The temporal dimension of differenced Normalized Burn Ratio (dNBR) fire/burn severity studies: The case of the large 2007 Peloponnese wildfires in Greece. *Remote Sens. Environ.* **2010**, *114*, 2548–2563.
23. Haest, B.; Thoonen, G.; Borre, J.V.; Spanhove, T.; Delalieux, S.; Bertels, L.; Kooistra, L.; Scheunders, P. An object-based approach to quantity and quality assessment of heathland habitats in the framework of NATURA 2000 using hyperspectral airborne AHS images. *Int. Arch. Photogramm. Remote Sens. Spat. Inf. Sci.* **2010**. Available online: http://www.isprs.org/proceedings/XXXVIII/4-C7/pdf/Haest_211.pdf (accessed on 13 February 2014).
24. Veraverbeke, S.; Somers, B.; Gitas, I.; Katagis, T.; Polychronaki, A.; Goossens, R. Spectral mixture analysis to assess post-fire vegetation regeneration using Landsat Thematic Mapper imagery: Accounting for soil brightness variation. *Int. J. Appl. Earth Obs. Geoinf.* **2012**, *14*, 1–11.
25. Key, C.H.; Benson, N.C. Landscape Assessment: Ground Measure of Severity, the Composite Burn Index, and Remote Sensing of Severity, the Normalized Burn Index. In *FIREMON: Fire Effects Monitoring and Inventory System*; Lutes, D., Keane, R., Caratti, J., Key, C.H., Benson, N.C., Sutherland, S., Gangi, L., Eds.; Rocky Mountains Research Station, USDA Forest Service: Fort Collins, CO, USA, 2005.
26. Van Wagtendonk, J.W.; Root, R.R.; Key, C.H. Comparison of AVIRIS and Landsat ETM+ detection capabilities for burn severity. *Remote Sens. Environ.* **2004**, *92*, 397–408.
27. Chuvieco, E. *Remote Sensing of Large Wildfires in the European Mediterranean Basin*; Springer: Berlin/Heidelberg, Germany, 1999; p. 212.
28. De Santis, A.; Chuvieco, E. Burn severity estimation from remotely sensed data: Performance of simulation *versus* empirical models. *Remote Sens. Environ.* **2007**, *108*, 422–435.
29. De Santis, A.; Chuvieco, E.; Vaughan, P.J. Short-term assessment of burn severity using the inversion of PROSPECT and GeoSail models. *Remote Sens. Environ.* **2009**, *113*, 126–136.
30. Lhermitte, S.; Verbesselt, J.; Verstraeten, W.W.; Veraverbeke, S.; Coppin, P. Assessing intra-annual vegetation regrowth after fire using the pixel based regeneration index. *ISPRS J. Photogramm. Remote Sens.* **2011**, *66*, 17–27.
31. Murphy, K.A.; Reynolds, J.H.; Koltun, J.M. Evaluating the ability of the differenced Normalized Burn Ratio (dNBR) to predict ecologically significant burn severity in Alaskan boreal forests. *Int. J. Wildland Fire* **2008**, *17*, 490–499.

32. French, N.H.F.; Kasischke, E.S.; Hall, R.J.; Murphy, K.A.; Verbyla, D.L.; Hoy, E.E.; Allen, J.L. Using Landsat data to assess fire and burn severity in the North American boreal forest region: An overview and summary of results. *Int. J. Wildland Fire* **2008**, *17*, 443–462.
33. De Santis, A.; Asner, G.P.; Vaughan, P.J.; Knapp, D.E. Mapping burn severity and burning efficiency in California using simulation models and Landsat imagery. *Remote Sens. Environ.* **2010**, *114*, 1535–1545.
34. Veraverbeke, S.; Hook, S. Evaluating spectral indices and spectral mixture analysis for assessing fire severity, combustion completeness, and carbon emissions. *Int. J. Wildland Fire* **2013**, *22*, 707–720.
35. Kokaly, R.F.; Rockwell, B.W.; Haire, S.L.; King, T.V.V. Characterization of post-fire surface cover, soils, and burn severity at the Cerro Grande Fire, New Mexico, using hyperspectral and multispectral remote sensing. *Remote Sens. Environ.* **2007**, *106*, 305–325.
36. Robichaud, P.R.; Lewis, S.A.; Laes, D.Y.M.; Hudak, A.T.; Kokaly, R.F.; Zamudio, J.A. Postfire soil burn severity mapping with hyperspectral image unmixing. *Remote Sens. Environ.* **2007**, *108*, 467–480.
37. Lewis, S.A.; Lentile, L.B.; Hudak, A.T.; Robichaud, P.R.; Morgan, P.; Bobbitt, M.J. Mapping ground cover using hyperspectral remote sensing after the 2003 Simi and old wildfires in Southern California. *Fire Ecol.* **2007**, *3*, 109–128.
38. Smith, A.M.S.; Lentile, L.B.; Hudak, A.T.; Morgan, P. Evaluation of linear spectral unmixing and ΔNBR for predicting post-fire recovery in a North American ponderosa pine forest. *Int. J. Remote Sens.* **2007**, *28*, 5159–5166.
39. Smith, A.M.S.; Wooster, M.J.; Drake, N.A.; Dipotso, F.M.; Falkowski, M.J.; Hudak, A.T. Testing the potential of multi-spectral remote sensing for retrospectively estimating fire severity in African Savannahs. *Remote Sens. Environ.* **2005**, *97*, 92–115.
40. Quintano, C.; Fernández-Manso, A.; Roberts, D.A. Multiple Endmember Spectral Mixture Analysis (MESMA) to map burn severity levels from Landsat images in Mediterranean countries. *Remote Sens. Environ.* **2013**, *136*, 76–88.
41. Veraverbeke, S.; Harris, S.; Hook, S. Evaluating spectral indices for burned area discrimination using MODIS/ASTER (MASTER) airborne simulator data. *Remote Sens. Environ.* **2011**, *115*, 2702–2709.
42. Chafer, C.; Noonan, M.; Macnaught, E. The post-fire measurement of fire severity and intensity in the Christmas 2001 Sydney wildfires. *Int. J. Wildland Fire* **2004**, *13*, 227–240.
43. Hammill, K.A.; Bradstock, R.A. Remote sensing of fire severity in the Blue Mountains: Influence of vegetation type and inferring fire intensity. *Int. J. Wildland Fire* **2006**, *15*, 213–226.
44. Harris, S.; Veraverbeke, S.; Hook, S. Evaluating spectral indices for assessing fire severity in chaparral ecosystems (Southern California) using MODIS/ASTER (MASTER) airborne simulator data. *Remote Sens.* **2011**, *3*, 2403–2419.
45. Chuvieco, E.; Martín, M.P.; Palacios, A. Assessment of different spectral indices in the red-near-infrared spectral domain for burned land discrimination. *Int. J. Remote Sens.* **2002**, *23*, 5103–5110.

46. Smith, A.M.S.; Drake, N.A.; Wooster, M.J.; Hudak, A.T.; Holden, Z.A.; Gibbons, C.J. Production of Landsat ETM+ reference imagery of burned areas within Southern African savannahs: Comparison of methods and application to MODIS. *Int. J. Remote Sens.* **2007**, *28*, 2753–2775.
47. Trigg, S.; Flasse, S. An evaluation of different bi-spectral spaces for discriminating burned shrub-savannah. *Int. J. Remote Sens.* **2001**, *22*, 2641–2647.
48. Bastarrika, A.; Chuvieco, E.; Martín, M.P. Mapping burned areas from Landsat TM/ETM+ data with a two-phase algorithm: Balancing omission and commission errors. *Remote Sens. Environ.* **2011**, *115*, 1003–1012.
49. Epting, J.; Verbyla, D.; Sorbel, B. Evaluation of remotely sensed indices for assessing burn severity in interior Alaska using Landsat TM and ETM+. *Remote Sens. Environ.* **2005**, *96*, 328–339.
50. Hoy, E.E.; French, N.H.F.; Turetsky, M.R.; Trigg, S.N.; Kasischke, E.S. Evaluating the potential of Landsat TM/ETM+ imagery for assessing fire severity in Alaskan black spruce forests. *Int. J. Wildland Fire* **2008**, *17*, 500–514.
51. Ju, J.; Roy, D.P. The availability of cloud-free Landsat ETM+ data over the conterminous United States and globally. *Remote Sens. Environ.* **2008**, *112*, 1196–1211.
52. Boelman, N.T.; Rocha, A.V.; Shaver, G.R. Understanding burn severity sensing in Arctic tundra: Exploring vegetation indices, suboptimal assessment timing and the impact of increasing pixel size. *Int. J. Remote Sens.* **2011**, *32*, 7033–7056.
53. Verbyla, D.L.; Kasischke, E.S.; Hoy, E.E. Seasonal and topographic effects on estimating fire severity from Landsat TM/ETM+ data. *Int. J. Wildland Fire* **2008**, *17*, 527–534.
54. Veraverbeke, S.; Verstraeten, W.W.; Lhermitte, S.; Goossens, R. Illumination effects on the differenced Normalized Burn Ratio's optimality for assessing fire severity. *Int. J. Appl. Earth Obs. Geoinf.* **2010**, *12*, 60–70.
55. Veraverbeke, S.; Lhermitte, S.; Verstraeten, W.W.; Goossens, R. Evaluation of pre/post-fire differenced spectral indices for assessing burn severity in a Mediterranean environment with Landsat Thematic Mapper. *Int. J. Remote Sens.* **2011**, *32*, 3521–3537.
56. De Santis, A.; Chuvieco, E., GeoCBI: A modified version of the Composite Burn Index for the initial assessment of the short-term burn severity from remotely sensed data. *Remote Sens. Environ.* **2009**, *113*, 554–562.
57. De Blust, G., Ed. *Heathlands in a Changing Society. Abstracts and Excursion Guide. 9th European Heathland Workshop, Belgium, 13th–17th September 2005*; Institute of Nature Conservation: Brussels, Belgium, 2005.
58. Hudak, A.T.; Morgan, P.; Bobbitt, M.J.; Smith, A.M.S.; Lewis, S.A.; Lentile, L.B.; Robichaud, P.R.; Clark, J.T.; McKinley, R.A. The relationship of multispectral satellite imagery to immediate fire effects. *Fire Ecol.* **2007**, *3*, 64–90.
59. Keeley, J. Fire severity and plant age in postfire resprouting of woody plants in sage scrub and chaparral. *Madrono* **2006**, *53*, 373–379.
60. Holden, Z.A.; Morgan, P.; Smith, A.M.S.; Vierling, L. Beyond Landsat: A comparison of four satellite sensors for detecting burn severity in ponderosa pine forests of the Gila Wilderness, NM, USA. *Int. J. Wildland Fire* **2010**, *19*, 449.
61. Schläpfer, D.; Schaepman, M.; Bojinski, S.; Börner, A. Calibration and validation concept for the airborne prism experiment (APEX). *Can. J. Remote Sens.* **2000**, *26*, 455–465.

62. Biesemans, J.; Sterckx, S.; Knaeps, E.; Vreys, K.; Adriaensen, S.; Hooyberghs, J.; Meuleman, K.; Kempeneers, P.; Deronde, B.; Everaerts, J.; *et al.* Image Processing Workflows for Airborne Remote Sensing. In Proceedings 5th EARSeL Workshop on Imaging Spectroscopy, Bruges, Belgium, 23–25 April 2007; pp. 1–14.
63. Berk, A.; Anderson, G.P.; Acharya, P.K.; Chetwynd, J.H.; Bernstein, L.S.; Shettle, E.P.; Matthew, M.W.; Adler-Golden, S.M. *Modtran4 USER'S MANUAL*; Air Force Materiel Command, Hanscom AFB, Bedford, MA, USA, 2001.
64. Thoonen, G.; Spanhove, T.; Vanden Borre, J.; Scheunders, P. Classification of heathland vegetation in a hierarchical contextual framework. *Int. J. Remote Sens.* **2013**, *34*, 96–111.
65. Tucker, C. Red and photographic infrared linear combinations for monitoring vegetation. *Remote Sens. Environ.* **1979**, *8*, 127–150.
66. Qi, J.; Chehbouni, A.; Huete, A.R.; Kerr, Y.H.; Sorooshian, S. A modified soil adjusted vegetation index. *Remote Sens. Environ.* **1994**, *48*, 119–126.
67. Huete, A. A soil-adjusted vegetation index (SAVI). *Remote Sens. Environ.* **1988**, *25*, 295–309.
68. Pinty, B.; Verstraete, W.W. GEMI: A non-linear index to monitor global vegetation from satellites. *Vegetatio* **1992**, *101*, 15–20.
69. Pereira, J.M.C. A comparative evaluation of NOAA/AVHRR vegetation indexes for burned surface detection and mapping. *IEEE Trans. Geosci. Remote Sens.* **1999**, *37*, 217–226.
70. Huete, A.; Didan, K.; Miura, T.; Rodriguez, E.; Gao, X.; Ferreira, L. Overview of the radiometric and biophysical performance of the MODIS vegetation indices. *Remote Sens. Environ.* **2002**, *83*, 195–213.
71. Pleniou, M.; Koutsias, N. Sensitivity of spectral reflectance values to different burn and vegetation ratios: A multi-scale approach applied in a fire affected area. *ISPRS J. Photogramm. Remote Sens.* **2013**, *79*, 199–210.
72. Holden, Z.A.; Smith, A.M.S.; Morgan, P.; Rollins, M.G.; Gessler, P.E. Evaluation of novel thermally enhanced spectral indices for mapping fire perimeters and comparisons with fire atlas data. *Int. J. Remote Sens.* **2005**, *26*, 4801–4808.
73. Lasaponara, R. Estimating spectral separability of satellite derived parameters for burned areas mapping in the Calabria region by using SPOT-Vegetation data. *Ecol. Model.* **2006**, *196*, 265–270.
74. Miller, J.D.; Thode, A.E. Quantifying burn severity in a heterogeneous landscape with a relative version of the delta Normalized Burn Ratio (dNBR). *Remote Sens. Environ.* **2007**, *109*, 66–80.
75. Allen, J.L.; Sorbel, B. Assessing the differenced Normalized Burn Ratio's ability to map burn severity in the boreal forest and tundra ecosystems of Alaska's national parks. *Int. J. Wildland Fire* **2008**, *17*, 463.
76. López-García, M.J.; Caselles, V. Mapping burns and natural reforestation using Thematic Mapper data. *Geocarto Int.* **1991**, *6*, 31–37.
77. Pereira, J.M.C.; Sá, A.C.L.; Sousa, A.M.O.; Silva, J.M.N.; Santos, T.N.; Carreiras, J.M.B. Spectral Characterisation and Discrimination of Burnt Areas. In *Remote Sensing of Large Wildfires in the European Mediterranean Basin*; Springer-Verlag: Berlin, Germany, 1999; pp. 123–138.

78. Gao, B.-C.; Goetz, A.F.H. Extraction of dry leaf spectral features from reflectance spectra of green vegetation. *Remote Sens. Environ.* **1994**, *47*, 369–374.
79. Gao, B.-C. NDWI—A Normalized Difference Water Index for remote sensing of vegetation liquid water from space. *Remote Sens. Environ.* **1996**, *58*, 257–266.
80. Jacquemoud, S.; Verhoef, W.; Baret, F.; Bacour, C.; Zarco-Tejada, P.J.; Asner, G.P.; Fran ϙis, C.; Ustin, S.L. PROSPECT+SAIL models: A review of use for vegetation characterization. *Remote Sens. Environ.* **2009**, *113*, S56–S66.
81. Bacour, C.; Baret, F.; Jacquemoud, S. Information Content of HyMap Hyperspectral Imagery. In Proceedings of 1st International Symposium on Recent Advances in Quantitative Remote Sensing, Valencia, Spain, 27 September–1 October 2002; pp. 503–508.
82. Lewis, S.A.; Hudak, A.T.; Ottmar, R.D.; Robichaud, P.R.; Lentile, L.B.; Hood, S.M.; Cronan, J.B.; Morgan, P. Using hyperspectral imagery to estimate forest floor consumption from wildfire in boreal forests of Alaska, USA. *Int. J. Wildland Fire* **2011**, *20*, 255–271.
83. Somers, B.; Asner, G.P.; Tits, L.; Coppin, P. Endmember variability in Spectral Mixture Analysis: A review. *Remote Sens. Environ.* **2011**, *115*, 1603–1616.
84. Baldridge, A.M.; Hook, S.J.; Grove, C.I.; Rivera, G. The ASTER spectral library version 2.0. *Remote Sens. Environ.* **2009**, *113*, 711–715.